Upper oceanic response to tropical cyclone Phailin in the Bay of Bengal using a coupled atmosphere-ocean model

Kumar Ravi Prakash[1] · Vimlesh Pant[1]

Abstract A numerical simulation of very severe cyclonic storm 'Phailin', which originated in southeastern Bay of Bengal (BoB) and propagated northwestward during 10–15 October 2013, was carried out using a coupled atmosphere-ocean model. A Model Coupling Toolkit (MCT) was used to make exchanges of fluxes consistent between the atmospheric model 'Weather Research and Forecasting' (WRF) and ocean circulation model 'Regional Ocean Modelling System' (ROMS) components of the 'Coupled Ocean-Atmosphere-Wave-Sediment Transport' (COAWST) modelling system. The track and intensity of tropical cyclone (TC) Phailin simulated by the WRF component of the coupled model agrees well with the best-track estimates reported by the India Meteorological Department (IMD). Ocean model component (ROMS) was configured over the BoB domain; it utilized the wind stress and net surface heat fluxes from the WRF model to investigate upper oceanic response to the passage of TC Phailin. The coupled model shows pronounced sea surface cooling (2–2.5 °C) and an increase in sea surface salinity (SSS) (2–3 psu) after 06 GMT on 12 October 2013 over the northwestern BoB. Signature of this surface cooling was also observed in satellite data and buoy measurements. The ocean-ic mixed layer heat budget analysis reveals relative roles of different oceanic processes in controlling the mixed layer temperature over the region of observed cooling. The heat budget highlighted major contributions from horizontal advection and vertical entrainment processes in governing the mixed

layer cooling (up to -0.1 °C h^{-1}) and, thereby, reduction in sea surface temperature (SST) in the northwestern BoB during 11–12 October 2013. During the post-cyclone period, the net heat flux at surface regained its diurnal variations with a noon-time peak that provided a warming tendency up to 0.05 °C h^{-1} in the mixed layer. Clear signatures of TC-induced upwelling are seen in vertical velocity (about 2.5×10^{-3} m s^{-1}), rise in isotherms and isohalines along 85–88° E longitudes in the northwestern BoB. The study demonstrates that a coupled atmosphere-ocean model (WRF + ROMS) serves as a useful tool to investigate oceanic response to the passage of cyclones.

Keywords Tropical cyclone · Phailin · Bay of Bengal · Upwelling · WRF · ROMS · COAWST model

1 Introduction

The upper ocean, defined as the first few hundred meters below the sea surface, interacts dynamically and thermo-dynamically with tropical cyclones (TCs) through the exchange of heat and moisture fluxes across the air-sea interface. Strong wind speed intensifies TC that leads to an increase in the evaporation rate and provides excess of latent heat flux to sustain the TC. Understanding the thermohaline structure of the upper ocean and its response to TC is crucial for timely and accurate prediction of TC intensity (Bender and Ginis 2000; Ali et al. 2007; Lin et al. 2009; Kaplan et al. 2010; Yablonsky and Ginis 2013). High wind conditions produce strong turbulent mixing in the upper ocean; this leads to a decrease in the sea surface temperature (SST) due to entrain-ment of the cooler waters from the thermocline into the mixed layer (Price 1981; Bender et al. 1993). Further, the cyclonic wind stress results into divergence at surface that leads to the

✉ Vimlesh Pant
vimlesh@iitd.ac.in; vimleshpant@gmail.com

[1] Centre for Atmospheric Sciences, Indian Institute of Technology Delhi, Hauz Khas, New Delhi 110016, India

Ekman transport (Ekman 1905) radially away from the centre of the cyclone. This Ekman transport then generates upward vertical velocity, i.e. Ekman suction (Stommel 1958), leading to cyclone-induced upwelling that reduces SST. Cooling of sea surface acts as a negative feedback mechanism on TC intensity (Schade and Emanuel 1999; Bosart et al. 2000; Chan et al. 2001; Lin et al. 2005). Key factors for uncertainties in forecasting TC intensity are storm inner core dynamics, structure of the atmospheric synoptic scale environment and interactions with upper-ocean layers (Emanuel 1999; Marks and Shay 1998). This pivotal role of the ocean-atmosphere interaction arises from the fact that TCs primarily draw their energy from evaporation at the ocean surface (Riehl 1950). TCs generally cool the ocean surface by several degrees along their track (Leipper 1967; Shay et al. 1992; Cione et al. 2000; D'Asaro 2003). While higher ambient SSTs provide the potential for stronger TCs, cyclone intensity is most sensitive to SST cooling under the storm eye (Schade 2000). This cooling reduces the total enthalpy flux provided to the atmosphere and inhibits the cyclone intensification (Cione and Uhlhorn 2003). Several studies have illustrated the influence of subsurface oceanic background conditions on the TC-induced SST signature (Shay et al. 2000; Cione and Uhlhorn 2003; Jacob and Shay 2003; Shay and Brewster 2010; Lloyd and Vecchi 2011; Vincent et al. 2012a, b). Vincent et al. (2012a, b) observed that the widely varying upper-ocean pre-cyclone stratification could modulate TC-induced cooling amplitude by up to an order of magnitude for a given level of TC kinetic energy input to the upper ocean.

Bay of Bengal (BoB), a semi-enclosed basin in the North Indian Ocean, receives large freshwater flux due to excess precipitation over evaporation and river runoff that maintains strong haline stratification (Shenoi et al. 2002; Rao and Sivakumar 2003; Thadathil et al. 2007; Girishkumar et al. 2013; Pant et al. 2015). Stratified upper ocean leads to shallow mixed layer (<30 m) and warmer (>28 °C) SST in the BoB that makes it an active region for the formation of tropical cyclones (TCs), a destructive natural disaster. Alam et al. (2003) reported that almost 5% of the global TCs form over the BoB region. TCs in the BoB occur more frequently during the pre-monsoon (May–June) and post-monsoon (October–December) months. McPhaden et al. (2009) reported that conditions favourable for TC formation, such as higher SST (28–30 °C), thermodynamically unstable atmosphere and weak tropospheric wind shear, are present during the pre- and post-monsoon seasons in the BoB. While the warmer SST supplies energy to TC, the strong wind stress at sea surface associated with TC can overcome the barrier layer, the layer between bottom of the mixed layer and top of the thermocline, to mix the colder and saltier water into the mixed layer from below. This process leads to sea surface cooling (Price 1981; Behera et al. 1998; Subramanyam et al. 2005; Sengupta et al. 2007; Lloyd and

Vecchi 2011; Yablonsky and Ginis 2013), which can reduce the intensity of TC due to reduction in enthalpy fluxes to atmosphere (Emanuel 1999; Zhu and Zhang 2006; Cione and Uhlhorn 2003). Different processes such as advection of cold water, enthalpy flux to atmosphere and vertical processes (entrainment) within ocean operate to produce the cooling of the sea surface. However, their relative contributions may differ in cyclones over different oceanic regions. A number of studies have shown that about 70–80% of SST cooling resulted from vertical processes due to TC-induced upwelling, and enthalpy flux or horizontal advection contributes about 20% (Price 1981; Vincent et al. 2012a, b). The SST reduction associated with TC in the BoB has large spatial and temporal variability. As compared to pre-monsoon, the SST cooling due to TC was found to be lower during the post-monsoon season due to the presence of thick barrier layers and existence of thermal inversions (Sengupta et al. 2007; Neetu et al. 2012). However, the intense rainfall associated with TC may increase the near-surface stratification and, therefore, reduce the SST cooling (Jacob and Koblinsky 2007; Jourdain et al. 2013).

Along with SST cooling, observations in the BoB have shown an increase in sea surface salinity (SSS) (McPhaden et al. 2009; Maneesha et al. 2012; Vinayachandran et al. 2013) and increase in chlorophyll-a (Chl-a) concentrations (Nayak et al. 2001; Babin et al. 2004). The BoB shows lower biological productivity as compared to Arabian Sea due to strong haline stratification and lower coastal upwelling. Strong cyclonic wind stress under the TCs can provide enough upwelling motion to overcome the barrier of stratification and bring the nutrient-enriched waters near surface (Tummala et al. 2009). TC-induced upwelling of nutrients from subsurface to the sun-lit photic zone increases Chl-a, which is usually considered as a proxy to indicate the phytoplankton biomass associated with a phytoplankton bloom (Subrahmanyam et al. 2002; Babin et al. 2004; Lotliker et al. 2014). The increase in Chl-a can subsequently increase the primary productivity of oceans and affect fish population. Studies utilizing the remotely sensed ocean colour monitor (OCM) data have shown that the TC-induced Chl-a enhancement and SST cooling bear an inverse correlation (Lin and et al. 2003; Babin et al. 2004; Walker et al. 2005).

However, the lack of high temporal and spatial observations, particularly during the passage of TC, poses a difficult problem to resolve upper oceanic response. Therefore, the studies rely on measurements from nearby buoy or satellite data, which may have their own uncertainties during storm and cloudy conditions. In the present study, we used a coupled atmosphere-ocean model (Weather Research and Forecasting (WRF) + Regional Ocean Modelling System (ROMS)) as components of Coupled Ocean-Atmosphere-Wave-Sediment Transport (COAWST) modelling system to simulate TC 'Phailin' in the BoB that traversed from southeast to northwest BoB during 10–15 October 2013. Use of coupled model

enables us to estimate contributions of different oceanic processes in the mixed layer heat budget and the observed SST cooling during the TC Phailin.

The paper is organized in four sections. The first section provides detail introduction and literature survey in related field, the second section describes model details and methodology used, and the third section discusses the model simulations from atmospheric and oceanic model components of the coupled model and the effect of TC Phailin on upper oceanic water column through the mixed layer heat budget. Section 4 summarizes the findings of the study.

2 Data and methodology

2.1 Model details

The coupled model used in this study includes the atmospheric model 'Advanced Research Weather Research and Forecasting' (WRF-ARW) and the ocean model ROMS. The WRF-ARW and ROMS models along with a model coupler are components of the COAWST model. The COAWST modelling system, described in detail by Warner et al. (2010), allows exchange of variables between different model components using a model coupler to improve storm forecasting and investigate coastal processes and environment (Warner et al. 2010 and Warner et al. 2012). The COAWST modelling system has been applied in examining coastal processes at regional scales (Carniel et al. 2016; Ricchi et al. 2016; Olabarrieta et al. 2011 and Olabarrieta et al. 2012; Kumar and Nair 2015) and effect of a hurricane on the upper ocean (Zambon et al. 2014).

The ROMS model is a free-surface, hydrostatic, primitive equation ocean model used extensively for estuarine, coastal and basin-scale research applications (http:// www.myroms. org). The primitive equations in the ROMS model are evaluated using boundary-fitted orthogonal, curvilinear coordinates on a staggered Arakawa C grid (Arakawa and Lamb 1977). The model is discretized in the vertical over variable topography using a stretched terrain-following sigma coordinate system (Phillips 1957; Song and Haidvogel 1994; Haidvogel et al. 2000). ROMS has been widely used by the scientific community for diverse applications ranging from basin scale to the coastal and estuarine scales (Song and Haidvogel 1994, Haidvogel et al. 2000; Marchesiello et al. 2003; Chassignet et al. 2000). Momentum and scalar advection and diffusive processes are solved using transport equations, and an equation of state is used to compute the density field that accounts for temperature, salinity and suspended sediment contributions. The atmospheric model WRF-ARW (WRF version 3.7.1) is a non-hydrostatic, fully compressible atmospheric model with boundary layer physics schemes and a variety of physical parameterizations of sub-grid-scale

processes for predicting mesoscales and microscales of motion (Skamarock et al. 2005; Skamarock and Klemp 2008). WRF uses Arakawa C grid and predicts three-dimensional wind momentum components, surface pressure, dew point, precipitation, surface sensible and latent heat fluxes, longwave and shortwave radiative fluxes, relative humidity and air temperature on a sigma-pressure vertical coordinate grid. WRF has been used extensively for operational forecasts. It incorporates various physical processes including microphysics, cumulus parameterization, planetary boundary layer, surface layer, land surface and longwave and shortwave radiations, with multiple options available for each process. In the COAWST modelling system, WRF code is modified to provide an enhanced bottom roughness when computing the bottom stress over the ocean (Warner et al. 2010). The wave and sediment transport model components are not used in the present study.

The coupler used in COAWST modelling system is the Model Coupling Toolkit (MCT) (Larson et al. 2004; Jacob et al. 2005) that allows the transmission and transformation of various distributed data between component models using a parallel coupled approach. During model initialization, each model decomposes its own domain into sections that are distributed to processors assigned for that component. Each grid section on each processor initializes with MCT, and MCT identifies the distribution of model components on all the processors. MCT can then determine the grid distributions. During execution, each model fills its attribute vector to exchange prognostic variables through MCT to other models. The variables that are exchanged between each model are detailed by Warner et al. (2010).

2.2 Model configuration and experiment design

The configuration of COAWST modelling system used in this study comprised atmosphere and ocean models (WRF + ROMS) and the coupler MCT to investigate the thermodynamic response of upper ocean during the passage of TC Phailin. The WRF-ARW (version 3.7.1) used in COAWST configuration integrates the fully compressible, non-hydrostatic governing equations on a terrain-following vertical coordinate system. It used physics parameterization schemes for handling surface radiation fluxes, boundary layer processes and precipitation processes. The Monin-Obukhov surface layer parameterization (Monin and Obukhov 1954) was used. NOAH land surface scheme was used in the model. Cloud-interactive shortwave radiation scheme from Dudhia (1989), rapid radiation transfer model (RRTM) for longwave radiation (Mlawer et al. 1997) and the Yonsei University planetary boundary layer (YSU PBL) explained by Noh et al. (2003) were used. The atmospheric and land surface layer models calculate exchange coefficients and surface fluxes off the land or ocean surface and pass them to the YSU PBL at every time step (Hong et al. 2006). The WRF single-moment

(WSM) six-class moisture microphysics scheme by Hong and Lim (2006) represents grid-scale precipitation processes (vapour, cloud, rain, snow, ice and graupel), and the Kain (2004) cumulus scheme represents sub-grid-scale convection and cloud detrainment. The ocean circulation model ROMS includes various accurate, high-order numerical schemes for sub-grid-scale advection and diffusion. The K-profile parameterization (KPP) mixing scheme formulation explained in Large et al. (1994) was used for the vertical turbulent mixing.

Model domains of both atmosphere (WRF-ARW) and ocean (ROMS) models used in this study as part of COAWST modelling system are shown in Fig. 1. The WRF model was used over the North Indian Ocean domain with two-way nested configuration (Michalakes et al. 2005) that featured a 27 km outer fixed domain (65–105° E, 1–34° N) with a movable inner domain (1188 km × 1188 km) of 9-km horizontal grid spacing. In the vertical, the model was discretized by 30 sigma levels. WRF was initialized with National Centre for Environmental Prediction (NCEP) Final Analysis (FNL) data on 10 October 2013 at 00 GMT. Lateral boundary conditions were supplied from FNL data at 6-h interval. Simulations were performed for the period of 10–15 October 2013. For the moving inner domain, repositioning over the outer domain is calculated every 30-min interval to better capture the centre of TC, i.e. the minimum surface pressure.

The ROMS ocean model domain covers the BoB region between 75° E–97° E and 7° N–29° N with uniform zonal and meridional horizontal grid spacings of 0.125° and 40 terrain-following vertical levels (Fig. 1). Lateral boundary in the configured ROMS model was closed in the north and open in the west, east and south. The ROMS model was also initialized from the same period as that of WRF-ARW model, i.e. 00 GMT on 10 October 2013. The oceanic initial and lateral open boundary

conditions in the ROMS model were derived from the 'Estimating the Circulation & Climate of the Ocean' (ECCO2) data. Ocean bathymetry was derived from ETOPO2 (2-min gridded global relief data). Variables exchanged between the two-way coupled WRF and ROMS models, through the MCT coupler, are shown in Fig. 2. The exchanged variables from WRF to ROMS model were zonal and meridional components of surface wind (u_{wind}, v_{wind}), atmospheric surface pressure (P_{atm}), relative humidity (RH), shortwave (SW_{rad}) and longwave (LW_{rad}) radiation, surface air temperature (T_{air}), cloud and rain rate. The ocean model uses these parameters in the COARE algorithm (Fairall et al. 1996) to compute the ocean surface stresses and ocean surface net heat fluxes (Warner et al. 2010). Variables were exchanged between the WRF and ROMS models at every 600-s interval. SST updated in WRF by the ROMS model allows obtaining surface fluxes, which are better and consistent between the two models.

2.3 Mixed layer heat budget

We used a simplified version of the mixed layer heat balance, following Foltz and McPhaden (2009) and Vialard et al. (2008),

$$\frac{\partial T}{\partial t} = \frac{(Q\mathrm{net} - Q\mathrm{pen})}{\rho c_p h} - \left[u\frac{\partial T}{\partial x} + v\frac{\partial T}{\partial y} \right] - \frac{W\Delta T}{h} + \mathrm{residual}.$$

$$\text{(a)} \qquad \text{(b)} \qquad \qquad \text{(c)} \qquad \quad \text{(d)} \qquad \text{(e)}$$

$$(1)$$

The individual terms in Eq. (1) represent (a) temperature tendency, (b) net surface heat flux, (c) horizontal advection, (d) vertical entrainment and (e) residual term in units of degree Celsius per hour. The vertically average mixed layer temperature
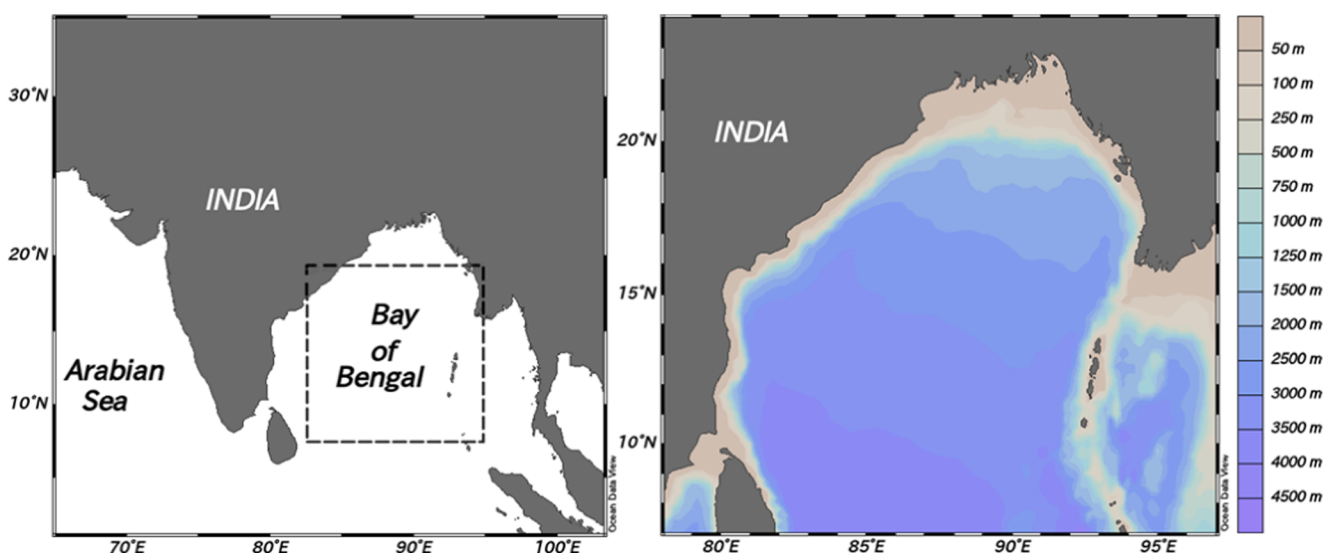

Fig. 1 *Left panel*: atmospheric model (WRF-ARW) with the outer fixed domain and inner moving domain (*broken line*) valid at initial condition 0000 GMT on 10 October 2013. *Right panel*: ocean model (ROMS) domain with bathymetry (m)
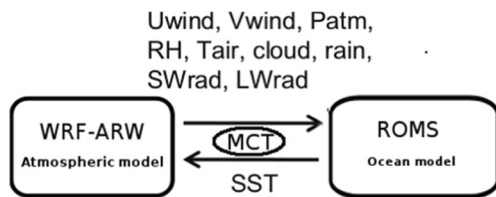
Fig. 2 Schematic showing the modelling components of the atmosphere-ocean coupled modelling system COAWST. Variables exchanged between atmospheric model (WRF-ARW) and ocean model (ROMS) are mentioned along with the Model Coupling Toolkit (MCT) coupler that allows the exchange of variables between the two models

is designated as T, ρ is the density of seawater, C_p is the specific heat capacity of seawater at constant pressure, t is the time, and h is the mixed layer depth (MLD). ΔT is the temperature difference between the mixed layer average temperature and the temperature just below the base of the mixed layer. Following Rao and Sivakumar (2003), the MLD is defined as the depth where the density is greater than surface value (5 m) by 0.125 kg m^{-3}. Latent (Q_L) and sensible (Q_S) heat fluxes were estimated by the WRF model. Q_{LW} is the longwave radiation flux at sea surface. Net surface shortwave radiation (Q_{SW}) was obtained from downwelling shortwave flux from WRF with correction for albedo at the sea surface. Q_{net} is the net surface heat flux term ($Q_{net} = Q_{SW} - Q_{Pen} + Q_{LW} + Q_L + Q_S$). Following Morel and Antoine (1994) and Sweeney et al. (2005), the penetrating short wave radiation (Q_{Pen}) below the mixed layer is estimated by $Q_{Pen} = 0.47 \, Q_{SW} \times [V_1 \, e - \mathrm{h}/\zeta_1 + V_2 \, e - h / \zeta_2]$, where ζ_1 and ζ_2 (in m) are the attenuation depths of long visible (ζ_1), short visible and ultraviolet (ζ_2) wavelengths and h is the MLD. V_1 and V_2 are the partitioning factors which are functions of chlorophyll concentration (Morel and Antoine 1994). The values of V_1, V_2, ζ_1 and ζ_2 were estimated from moderate-resolution imaging spectroradiometer (MODIS) 8-day composite Chl-a (mg m^{-3}) data using the method from Morel and Antoine (1994).

3 Results and discussion

3.1 Brief description of TC Phailin

TC Phailin that was recorded over the BoB basin in the North Indian Ocean made landfall near Gopalpur district of Odisha state at the east coast of India on 12 October 2013 at around 15:30 GMT. With the recorded maximum wind speeds of 200 km h^{-1}, Phailin was the strongest cyclone after the Orissa Super Cyclone that made landfall at Odisha coast in the year 1999 (Kumar and Nair 2015). This cyclone initially appeared as a low pressure area over north Andaman Sea on 7 October 2013 and converted into a depression at 00 GMT on 8 October centred near 12° N, 96° E (IMD Report 2013). The cyclone moved northwestward and intensified into a deep depression in the morning of 9 October. While moving in west–northwestward

direction, cyclone crossed Andaman islands at 09 GMT on 9 October. The cyclonic system moved slowly over east central BoB and intensified into a cyclonic storm (CS) named Phailin around 12 GMT on 9 October. Moving westward, the storm intensified into a severe cyclonic storm (SCS) at 03 GMT and further into a very severe cyclonic storm (VSCS) over the east central BoB around 06 GMT on 10 October. The storm intensified further and attained its maximum intensity around 03:00 GMT on 11 October. At this stage, it was located near (16.0° N, 88.5° E) with wind speed of 115 knots and central sea-level pressure (CSLP) of 940 hPa. Moving in northwestward direction, TC Phailin crossed east coast of India near Gopalpur around 17 GMT on 12 October 2013. After the landfall, the system moved north–northwestward for some time and finally north–northeastward. The storm weakened gradually into a SCS by 03 GMT and into CS around 06 GMT on 13 October. It further weakened into a deep depression by 12 GMT on 13 October and finally into a depression around 03 GMT on 14 October 2013 (Mandal et al. 2015).

3.2 Atmospheric model simulations

Figure 3 shows the WRF-ARW model-simulated track of TC Phailin with the position of eye, i.e. the pressure-minimum area in the inner domain of WRF model marked at every 3-h interval. For comparison, the India Meteorological Department (IMD) best track (IMD 2013) is also drawn with 3-hourly positions of the eye of TC Phailin. IMD (http://www.imd.gov.in/) is the principal government agency of India in matters relating to meteorology, seismology and related subjects. IMD takes meteorological observations over the country and provides current and forecast meteorological information for optimum operation of weather-sensitive activities. Date and time at every 12th hour are marked with a label on both the tracks for comparison of translational velocity of cyclone simulated with WRF-ARW with IMD best track. It is clear that the track simulated by the model is close to IMD best-track positions during most of the time of TC Phailin passage over the BoB. Model simulations are also compared with the two Ocean Moored buoy Network for Northern Indian Ocean (OMNI) buoys BD09 (17.86° N, 89.68° E) and BD10 (16.50° N, 88.00° E) in the vicinity of TC Phailin track (Venkatesan et al. 2013). Locations of buoys BD09 and BD10 are marked in Fig. 3. It is noteworthy that the simulated track was in close proximity of buoy BD10.

The comparisons of the along-track mean sea-level pressure (MSLP) and surface wind speed simulated by the WRF model with the IMD best estimates are shown in Fig. 4. The model simulates the intensity of TC Phailin realistically. The model-simulated along-track pressure well captured the decreasing trend from a pressure of 992 hPa on the model initial

Fig. 3 IMD best track (*red*) and WRF-ARW model-simulated track (*black*) for the tropical cyclone 'Phailin'. Position of the TC Phailin centre marked with *black* (simulated) and *red* (IMD) *dots* on the tracks at every 3 h and time is mentioned at every 12-h interval. Locations of two OMNI data buoys (BD09 and BD10) are marked with *blue dots*. hr in the labels stands for GMT hour
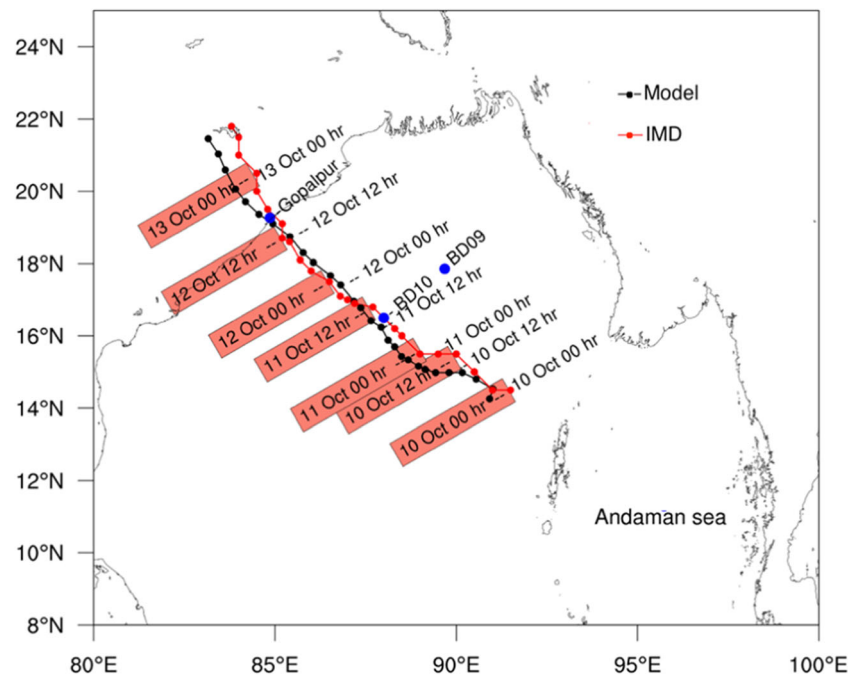
condition (00 GMT on 10 October) to the minimum pressure of 953 hPa at 06 GMT on 12 October. However, the IMD-estimated MSLP was higher by ~3 hPa at the model initial time and the minimum MSLP estimated value remained constant at 940 hPa from 03 GMT on 11 October to 15 GMT on 12 October. The increasing trend in the MSLP after 15 GMT on 12 October shows fairly good agreement between the model and the IMD data. The peak surface wind speed in model is weaker by ~8 m s^{-1} as compared to the IMD-estimated maximum sustained wind of 60 m s^{-1}, but the model is able to reproduce the trend of increasing wind speed from initial

condition to 00 GMT on 11 October and decreasing trend in wind speed starting from 03 GMT on 12 October. The correlations between the model and the IMD estimates for MSLP and wind speed were found to be 0.962 and 0.965, respectively.

Further, the WRF-ARW model-simulated wind speed was compared with the time series measurements at the two OMNI buoy locations BD09 (17.86° N, 89.68° E) and BD10 (16.50° N, 88.00° E) and the same is presented in Fig. 5. Model-simulated surface wind speed agrees well with the buoy observations. At the BD09 location, the WRF-ARW model

Fig. 4 WRF-ARW-simulated (*blue*) and IMD best estimated (*red*) along the track mean sea-level pressure (MSLP in hPa) in the *upper panel* and surface wind speed (in m s^{-1}) in the *lower panel*. hr stands for GMT hour
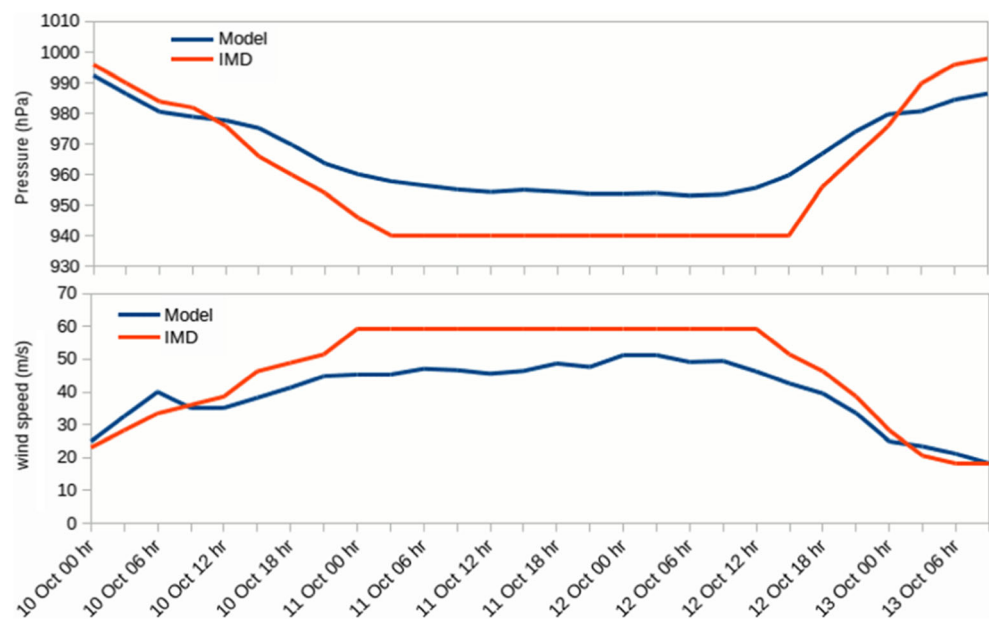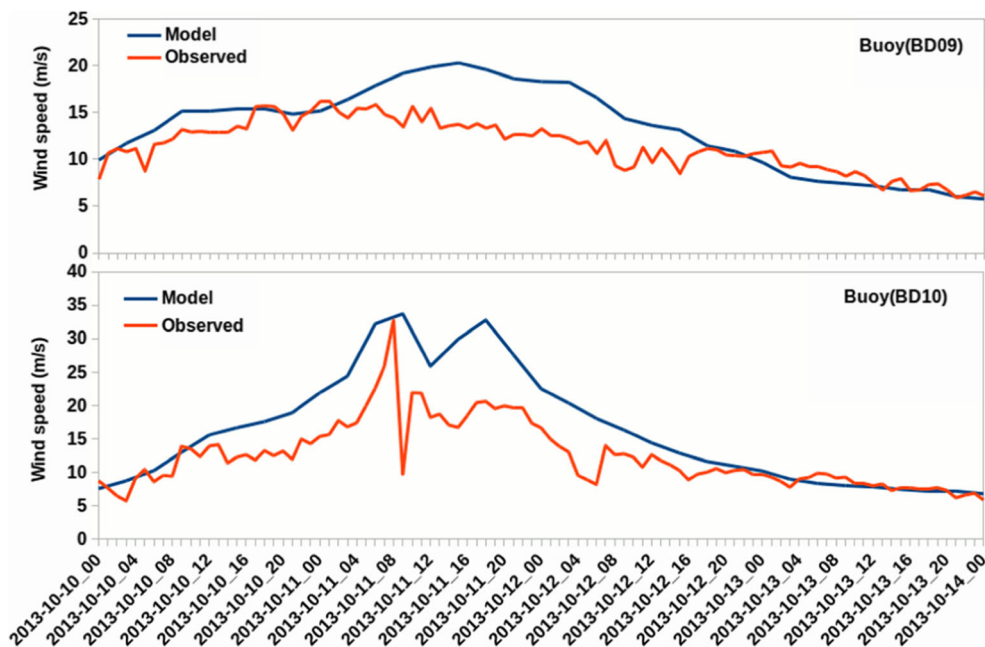
Fig. 5 WRF-ARW-simulated (*blue*) and observed (*red*) wind speed in metre per second at the data buoy locations BD09 (*upper panel*) and BD10 (*lower panel*). The *x*-axis labels indicate time in format year-month-day-hour (YYYY-MM-DD-HH in GMT)

started with a bias of ~2 m s^{-1} stronger winds in the initial condition. The model was able to capture the trends in wind speed such as the increasing trend from the initial time to the end of 10 October. However, the model predicted stronger wind speed at BD09 location during 11–12 October. Model-simulated winds agree very well with BD09 data after 13 October. At the BD10 location, where the buoy was in close proximity of the TC Phailin track, the model-simulated wind speed was close to the buoy measurements and followed the increasing (decreasing) trends in surface wind speed as the TC was approaching (departing) the buoy location. The model, however, could not realistically simulate the sharp decrease in wind speed from about 32 to 10 m s^{-1} within short time period of 1–2 h during 8–10 GMT on 11 October when the TC Phailin passed over BD10 location. It is worth to mention here that the BD10 buoy was within the eye and eyewall region of TC Phailin (Venkatesan et al. 2014). Therefore, BD10 recorded the typical surface wind pattern of increasing wind speed for the approaching TC, followed by rapid decrease in wind speed when the eye of TC was passing over the buoy location and further recovery of high wind speeds as the eyewall region of TC moved over the buoy location. With a marginal error in WRF-ARW-simulated track, these fast variations in surface wind could not be simulated over the location of buoy BD10.

3.3 Oceanic model simulations

The ROMS model simulations of the sea surface variables (currents, temperature and salinity) valid at 00 GMT of each day during 10–15 October 2013 are shown in Fig. 6. A comparison of sea surface temperature (SST) from model with the Advanced Very High-Resolution Radiometer (AVHRR)

satellite observations is also presented. However, due to non-availability of observed surface currents and salinity at high temporal resolution as that of the model (3 hourly), comparison of these model output variables was not attempted as they would be misrepresented if compared with daily mean values. The surface currents attain the cyclonic pattern in response to the cyclonic wind forcing from the WRF-ARW model (Fig. 6a). Cyclonic surface currents start strengthening from 1.0 m s^{-1} on 00 GMT of 10 October to the order of 1.8 m s^{-1} at 00 GMT on 12 October, which is the period of peak surface winds in WRF-ARW during the passage of TC Phailin. The structure of TC is seen as strong cyclonic currents with growth in size as the TC approached toward the coast during 11–12 October.

The SST from ROMS model shown in Fig. 6b was compared with the AVHRR SST (Fig. 6c) for corresponding 00 GMT of each day during 10–15 October 2013. As a consequence of the cyclonic wind stress generated divergence at the surface, the colder water upwelled and reduction in SST was observed in the vicinity of TC Phailin. The pronounced cooling with a decrease of 2–2.5 °C in SST was noticed during 12–13 October in both model and satellite observations. This reduction in SST persisted over mostly the same region with smaller spatial coverage in the northwestern BoB for the rest of the period of model simulations. Satellite observations also show the existence of colder surface waters with reduced spatial coverage up to 15 October over the same region. More details of the sea surface cooling in the northwestern BoB and underlying oceanic processes are given in the following section using the mixed layer heat budget analysis. Figure 6d shows the sea surface salinity (SSS) simulated by the ROMS model during
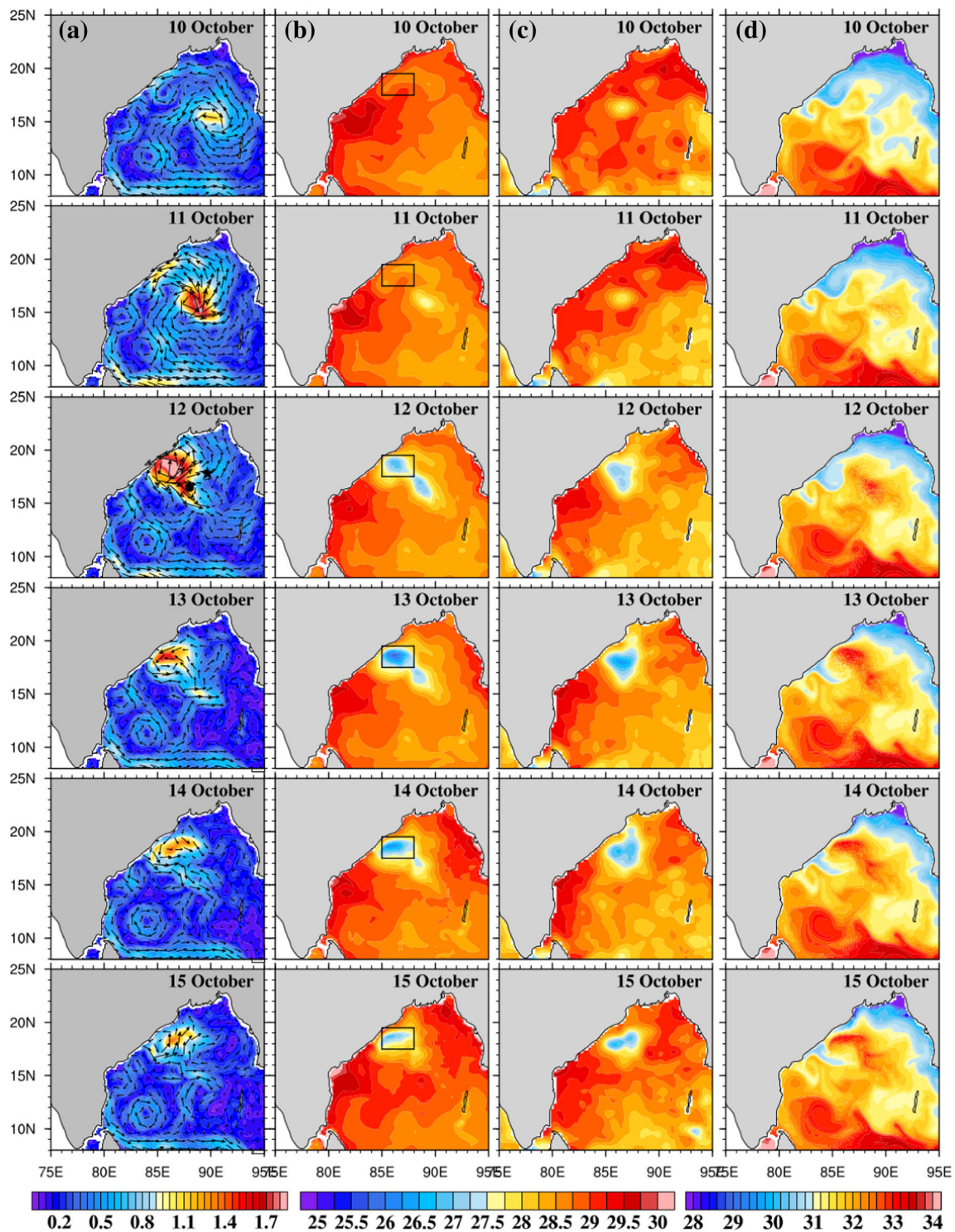
Fig. 6 **a** Model-simulated surface currents (m s^{-1}) at 00 GMT of each day, **b** model-simulated sea surface temperature (°C), **c** observed sea surface temperature from AVHRR and **d** model-simulated sea surface salinity (psu). The region selected for mixed layer heat budget analysis is marked with a *box* in the *second column*. Locations of BD09 and BD10 buoy are shown with a *solid star* and *circle*, respectively, in the *third-row first-column panel*

10–15 October at 00 GMT each day. Signatures of cyclone-induced upwelling are also seen in SSS patterns. In the vicinity of TC Phailin, increase in the SSS by about 2.5 psu was observed from 10 to 13 October.

Time series of temperature profiles from the ROMS model are compared at two buoy locations BD09 and BD10 and shown in Fig. 7. As seen in Fig. 3, the buoy BD09 is located about 200 km away from the TC track

Fig. 7 Time series of the temperature profile—at the buoy BD10 location [**a** model simulated and **b** observed] and at the buoy BD09 location [**c** model simulated and (**d** observed]
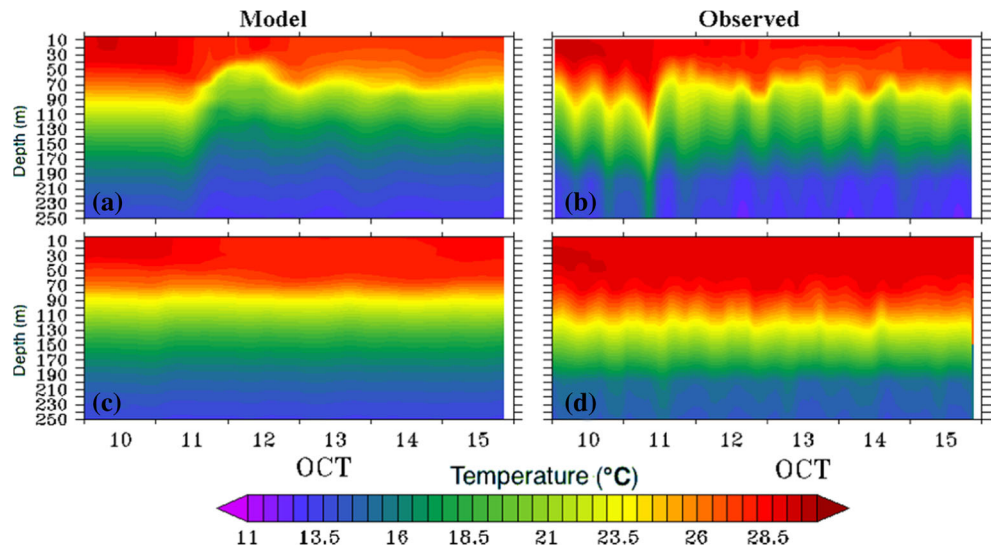
but well under the influence of cyclonic currents (Fig. 6a). The high-frequency variability in temperature seen in BD10 data (Fig. 7b) is, however, not present in model temperature profile (Fig. 7a), but the depth of 23 °C isotherm (D_{23}) shows good agreement with observations. Particularly, the shoaling of D_{23} after 12 October is well captured by model simulations at this location. Model is colder by 0.7 °C near surface. At the BD09 location, model-simulated temperature profile has 10–20 m shallower D_{23} and 0.5–0.9 °C colder near-surface temperatures as compared to observations, but the nearly constant behaviour is well represented.

3.4 Upper oceanic response in the region of surface cooling

Time series of temperature profile along with the MLD (dashed line) and D_{23} (solid line) are shown in the lower panel of Fig. 8. In order to plot the time series variation, area averaging of temperature is carried out over the region of observed surface cooling in the northwestern BoB (marked with a box in Fig. 6). Initial vertical structure of upper ocean found to have a shallow MLD (~15 m) on 10 October, before the arrival of TC Phailin over this region. As the TC approached, the MLD deepens to about 35 m during 11–12 October under the influence of strong winds in the northern flank of TC

Fig. 8 *Lower panel:* temporal variation of oceanic mixed layer depth (MLD in m) and depth of 23 °C isotherm (D_{23} in m). *Upper panel:* mixed layer heat budget terms (in °C h^{-1}) calculated using ROMS model simulations over an area (marked with a *box* in Fig. 6) with signature of upwelling in northwestern BoB
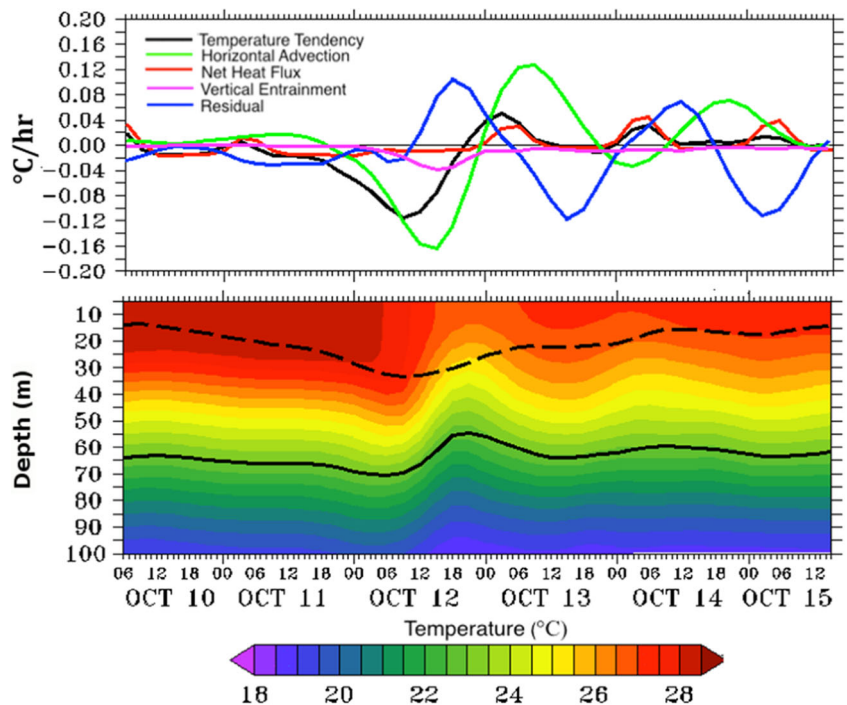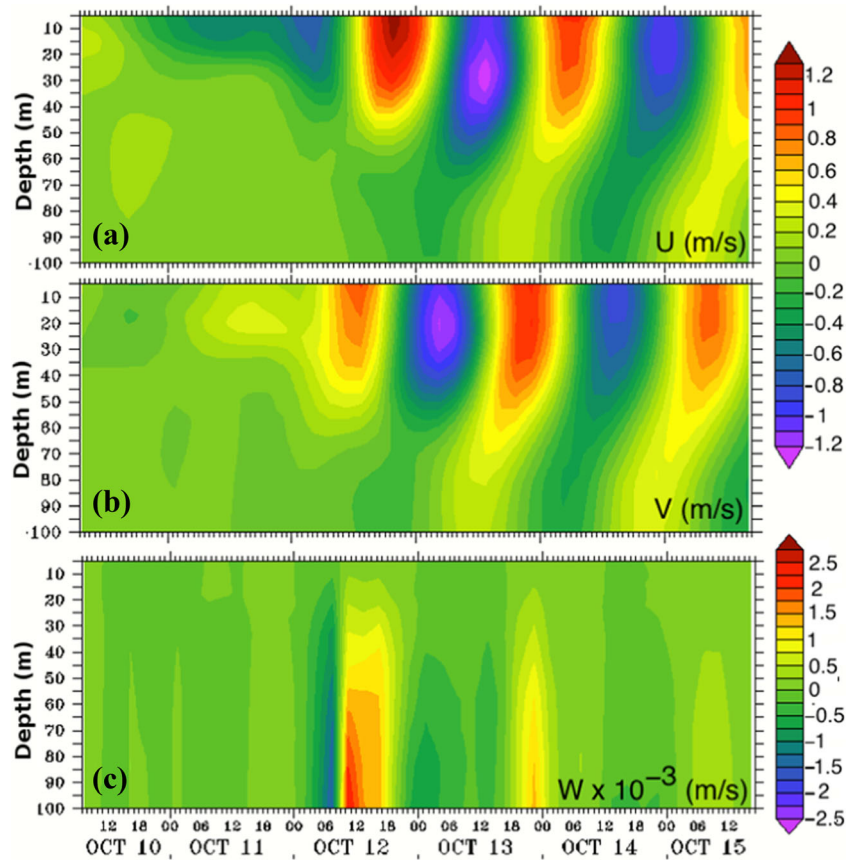
Fig. 9 Temporal variation in profiles of the zonal (*u*) and meridional (*v*) components of currents (in m s^{-1}) and vertical velocity (w × 10^{-3} m s^{-1}) averaged over the selected region (marked in Fig. 6) in northwestern BoB

Phailin. Cyclonic currents at the surface lead to shoaling (reduction in depth) of D$_{23}$ from 70 m at 06 GMT to 55 m at 18 GMT on 12 October.

In order to separate out the relative roles of different oceanic processes in controlling the sea surface cooling during the passage of cyclone over the marked region (see Fig. 6), we carried out the mixed layer heat budget analysis over the boxed region using the model results based on the methods described in Sect. 2.3. Time series of various terms of the mixed layer heat budget, i.e. temperature tendency, horizontal advection, net heat flux and vertical entrainment averaged over the selected region (marked in Fig. 6), were plotted in units of degree Celsius per hour and shown in the upper panel of Fig. 8. The unresolved processes, including turbulent mixing and diffusion, are represented by the residual term. Enhanced cooling of the mixed layer is evident from the temperature tendency curve, which shows rapid rate of negative tendency up to −0.1 °C h^{-1} from 06 GMT on 11 October to 18 GMT on 12 October. This cooling of the mixed layer may be attributed to the combined effect of horizontal advection, vertical entrainment from below the mixed layer and reduced net heat flux at the sea surface. Vertical entrainment term contributed up to −0.04 °C h^{-1} cooling rate within the selected region, whereas the advection of colder water to the selected region contributed up to −0.16 °C h^{-1} cooling rate. The noontime

peaks in the diurnal cycle of surface net heat flux were absent during 10–12 October due to inhibition of surface reaching shortwave radiation in presence of clouds associated with TC Phailin. The small magnitude of negative temperature tendency from residual term during the period of mixed layer cooling indicates the role of small scale mixing processes, which operates on the advected (horizontal and vertical) colder water. The magnitude of negative temperature tendency decreases after 09 GMT on 12 October as a result of positive tendency of residual term and decreasing negative tendency of horizontal advection during this period. During 13–15 October, the horizontal advection term changes its sign and primarily contributes to warming of the mixed layer, except for a few early morning hours of 14 October. Diurnal cycle in the net heat flux with the noontime peak was observed during 13–15 October, which also controls the mixed layer heat budget as reflected by the similar diurnal variations in the temperature tendency term. The diurnal cycle of warming tendency due to net heat flux during post-cyclone (13–15 October) period re-warms the sea surface. The periodicity in the temperature tendency from horizontal advection term may be associated with the advection of upwelled colder waters surfaced outside the selected region followed by the transport of warmer waters to this region as a result of increased net heat fluxes after the passage of TC Phailin. The noticeable larger

magnitude of residual term after 12 GMT on 12 October follows the variations in MLD and D_{23}. While the MLD progressively reduces from 35 to <20 m, D23 deepens from 55 to 65 m on 15 October as compared to 12 October. The small-scale unresolved processes represented by residual term contributed larger fraction in total temperature tendency during the period of shallower MLD. Therefore, the mixed layer heat budget analysis highlights dominant roles of horizontal advection and vertical entrainment during the cooling phase of mixed layer as the TC Phailin passes over the region of observed surface cooling in the northwestern BoB. After the passage of TC, the net heat flux, horizontal advection and residual terms dominate the temperature tendency of the mixed layer.

3.5 TC Phailin-induced upwelling

The profiles of the zonal (u), meridional (v) and vertical (w) components of currents averaged over the selected region (marked in Fig. 6) in the northwestern BoB are plotted in Fig. 9. The near-surface (up to 30 m from the sea surface) u-component of currents shows alternate negative (westward) and positive (eastward) directions with time as the TC Phailin passed over the region. Surface currents were mostly westward on 10–11 October when the TC was approaching from the southeast direction and reversed to have strong (up to 1.2 m s^{-1}) eastward component forced by the southeastern sector of the TC as also seen in Fig. 6. On the other hand,

the v-component was positive (northward) till 15 GMT on 12 October and thereafter changed to southward, which indicates crossing of TC Phailin over the region. The perturbations in u and v velocities sustaining after the passage of TC were associated with the inertial oscillations, which is in agreement with similar oscillations reported by Zambon et al. (2014) after the passage of Ivan cyclone. Vertical velocities at various depths plotted in Fig. 9c show interesting features during the passage of TC Phailin. Just before the landfall (i.e. 15:30 GMT on 12 October), maximum vertical velocities (w) of the order of 2.5×10^{-3} m s^{-1} were present at a depth of 80–100 m highlighting the cyclone-induced upwelling. However, the magnitude of w decreased toward the surface at the same time. For a short period of time before the arrival of TC over the region, there was a negative w-component at 70–100-m depth.

As a result of TC Phailin-induced surface Ekman divergence, shoaling of D_{23} (see Fig. 8) by 15–20 m was simulated by model on 12 October over the selected region in the northwestern BoB. This TC-induced upwelling contributed to the observed surface cooling by 2.2 °C in this region, which persisted for 2–3 days after the cyclone. Under suitable conditions following the passage of cyclones, the upwelled colder water can greatly enhance the primary productivity by increasing Chlorophyll-a (Chl-a) concentrations and lead to phytoplankton bloom (Nayak et al. 2001; Babin et al. 2004; Subrahmanyam et al. 2008), which can be monitored from satellite using ocean colour monitor (OCM). Upwelling of

Fig. 10 Daily mean profiles of salinity and temperature across the eastern (95° E) to western (82° E) transect in the northern BoB along the 19° N latitude on 13 October 2013
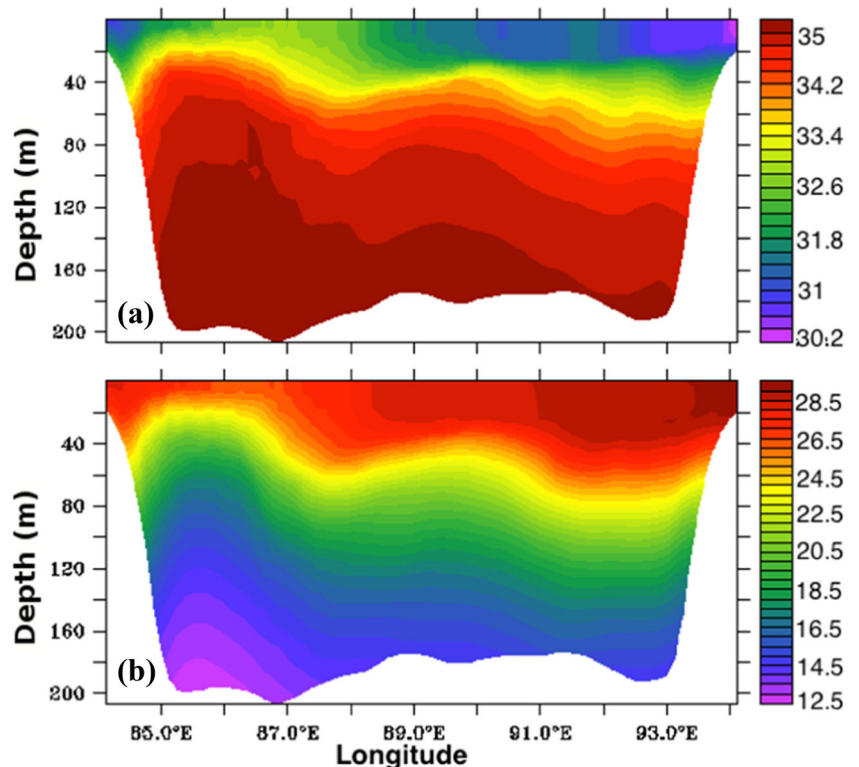
nutrients (e.g. nitrogen and phosphorous, iron) to the sun-lit photic zone and entrainment into the mixed layer under the influence of cyclonic wind stress give rise to the phytoplankton blooming. Because the upwelled water is colder, there is an established inverse relationship between SST and Chl-a enhancement (Babin et al. 2004; Subrahmanyam et al. 2008; Piontlovsky et al. 2012). Lotliker et al. (2014) used MODIS A satellite imageries to analyze biological productivity during the passage of TC Phailin. They reported the peak Chl-a concentrations of 0.65 mg m^{-3} on 12 October with an increase of 295% as compared to pre-cyclonic levels.

Model-simulated vertical profiles of salinity and temperature across the eastern (95° E) to western (82° E) BoB along the central latitude 19° N of the selected region for 13 October are shown in Fig. 10a, b, respectively. Signatures of TC-induced upwelling are also visible in both temperature and salinity profiles along 85–88° E longitudes. Subsurface high saline (>34 psu) waters from depths of 50–100 m rise to the surface layers and increase SSS by 2–3 psu as compared to either eastern or western longitudes to the region of upwelling. Similarly, the temperature contours rising to the sea surface along 85–88° E that cools the surface waters by 2–2.5 °C as compared to other longitudes with SST >27.5 °C.

4 Conclusions

The coupled atmosphere-ocean model using the atmospheric model 'WRF-ARW' and oceanic model 'ROMS' components of the 'COAWST' modelling system was used in this study to simulate the SCS Phailin that passed over the BoB during 10–15 October 2013. Performance of the coupled model was validated against observations for both atmospheric and oceanic parameters. Response of the oceanic mixed layer and upper oceanic thermohaline structure to the passage of TC Phailin was analyzed using model simulations and mixed layer heat budget. Coupled model-simulated track and intensity of TC Phailin were in good agreement with IMD best track and surface winds at two buoy locations. Both model and observations show pronounced cooling (about 2–2.5 °C) of the sea surface and increase in SSS (>2 psu) in the northwestern BoB after 12 October 2013. The mixed layer heat budget analysis revealed the dominant role of horizontal advection (−0.16 °C h^{-1}) and vertical entrainment (−0.04 °C h^{-1}) in governing the pronounced cooling of the mixed layer in the northwestern BoB during 11–12 October 2013. Reduction in the magnitude and diurnal periodicity of the net surface heat fluxes may be well recognized as a result of enhanced cloud cover during the passage of cyclone that inhibits the surface reaching shortwave radiation. The turbulent mixing and other small-scale processes (collectively represented by the residual term) mix the colder temperature anomaly within the mixed layer and lead to the reduction in SST. Model-simulated

vertical velocity up to 2.5×10^{-3} m s^{-1} indicated strong TC-induced upwelling over the region of observed surface cooling. Signatures of this upwelling were also seen in rising of isotherms (reduction in SST by 2–2.5 °C) and isohalines (increased SSS by 2–3 psu) along the 85–88° E longitudes in the northern BoB. The upwelled colder water, if enriched in nutrients, can enhance the primary productivity and lead to phytoplankton bloom. The study highlights the usefulness of a coupled atmosphere-ocean model for obtaining realistic simulations of atmospheric and oceanic parameters under the extreme weather conditions associated with a severe CS such as TC Phailin investigated in this study.

References

Alam MM, Hossain MA, Shafee S (2003) Frequency of Bay of Bengal cyclonic storms and depressions crossing different coastal zones. Inter J Climatol 23:1119–1125. doi:10.1002/joc.927

Ali MM, Jagadeesh PSV, Jain S (2007) Effects of eddies on Bay of Bengal cyclone intensity. Eos Trans AGU 88:93–95. doi:10.1029/ 2007EO080001

Babin SM, Carton JA, Dickey TD, Wiggert JD (2004) Satellite evidence of hurricane-induced phytoplankton blooms in an oceanic desert. J Geophys Res 109:C03043. doi:10.1029/2003JC001938

Behera SK, Deo AA, Salvekar PS (1998) Investigation of mixed layer response to Bay of Bengal cyclone using a simple ocean model. Meteorog Atmos Phys 65:77–91

Bender MA, Ginis I (2000) Real-case simulations of hurricane–ocean interaction using a high-resolution coupled model: effects on hurricane intensity. Mon Weather Rev 128:917–946. doi:10.1175/1520- 0493 (2000)128<0917:RCSOHO>2.0.CO;2

Bender MA, Ginis I, Kurihara Y (1993) Numerical simulations of the tropical cyclone-ocean interaction with a high-resolution coupled model. J Geophys Res 98:23245–23263

Bosart L, Velden CS, Bracken WE, Molinari J, Black PG (2000) Environmental influences on the rapid intensification of Hurricane Opal (1995) over the Gulf of Mexico. Mon Wea Rev 128:322–352

Carniel S, Barbariol F, Benetazzo A, Bonaldo D, Falcieri FM, Miglietta MM, Ricchi A, Sclavo M (2016) Scratching beneath the surface while coupling atmosphere, ocean and waves: analysis of a dense water formation event. Ocean Modeling 101:101–112

Chan JCL, Duan Y, Shay LK (2001) Tropical cyclone intensity change from a simple ocean-atmosphere coupled model. J Atmos Sci 58(2): 154–172

Cione JJ, Uhlhorn EW (2003) Sea surface temperature variability in hurricanes: implications with respect to intensity change. Mon Weather Rev 131:1783–1796. doi:10.1175//2562.1

Cione JJ, Black PG, Houston S (2000) Surface observations in the hurricane environment. Mon Wea Rev 128:1550–1561

Chassignet EP, Arango HG, Dietrich D, Ezer T, Ghil M, Haidvogel DB, Ma CC, Mehra A, Paiva AM, Sirkes Z (2000) DAMEE-NAB: the base experiments. Dyn Atmos Oceans 32:155–183

D'Asaro EA (2003) The ocean boundary layer under hurricane Dennis. J Phys Oceanogr 33:561–579

Dudhia J (1989) Numerical study of convection observed during the winter monsoon experiment using a mesoscale two dimensional model. J Atmos Sci 46:3077–3107

Ekman VW (1905) On the influence of the Earth's rotation on ocean currents. Arkiv for Matematik, Astronomi, och Fysik 2(11):1–52

Emanuel KA (1999) Thermodynamic control of hurricane intensity. Nature 401:665–669. doi:10.1038/44326

Fairall CW, Bradley EF, Rogers DP, Edson JB, Young GS (1996) Bulk parameterization of air–sea fluxes for Tropical Ocean Global Atmosphere Coupled Ocean-Atmosphere Response Experiment. J Geophys Res 101(C2):3747–3764

Foltz GR, McPhaden MJ (2009) Impact of barrier layer thickness on SST in the Central Tropical North Atlantic. J Clim 22:285–299. doi:10.1175/2008JCLI2308.1

Girishkumar MS, Ravichandran M, Han W (2013) Observed intraseasonal thermocline variability in the Bay of Bengal. J Geophys Res Oceans 118:3336–3349. doi: 10.1002/jgrc.20245

Hong SY, Noh Y, Dudhia J (2006) A new vertical diffusion package with explicit treatment of entrainment processes. Mon Weather Rev 134: 2318–2341

Haidvogel, DB, Arango, HG, Hedstrom, K, Beckmann, A, Malanotte-Rizzoli, P Shchepetkin, AF, (2000) Model evaluation experiments in the North Atlantic Basin: simulations in nonlinear terrain-following coordinates. Dyn Atmos Oceans 32, 239–281.

Hong SY, Lim JOJ (2006) The WRF single-moment 6-class microphysics scheme (WSM6). J Korean Meteor Soc 42(2):129–151

Jacob SD, Shay LK (2003) The role of oceanic mesoscale features on the tropical cyclone induced mixed layer response. J Phys Oceanogr 33: 649676

IMD Report (2013) Very severe cyclonic storm, PHAILIN over the Bay of Bengal (08–14 October 2013): a report. India Meteorological Department, Technical Report, October 2013

Jacob SD, Koblinsky C (2007) Effects of precipitation on the upper-ocean response to a hurricane. Mon Weather Rev 135:2207–2225

Jacob, R, Larson, J, Ong, E, (2005) M x N communication and parallel interpolation in CCSM using the model coupling toolkit. Preprint ANL/MCSP1225-0205. Mathematics and Computer Science Division, Argonne National Laboratory, 25 pp

Jourdain NC, Lengaigne M, Vialard J, Madec G, Menkes CE, Vincent EM, Samson G, Jullien Barnier B (2013) Observation-based estimates of ocean mixing inhibition by heavy rainfall under tropical cyclones. J Phys Oceanogr 43:205–221

Kain JS (2004) The Kain-Fritsch convective parameterization: an update. J Appl Meteor 43:170–181

Kaplan J, DeMaria MJ, Knaff A (2010) A revised tropical cyclone rapid intensification index for the Atlantic and eastern North Pacific Basins. Weather Forecast 25:220–241. doi:10.1175/2009WAF2222280.1

Kumar VS, Nair AM (2015) Inter-annual variations in wave spectral characteristics at a location off the central west coast of India. Ann Geophys 33:159–167. doi:10.5194/angeo-33-159-2015

Large GW, McWilliams JC, Doney SC (1994) Oceanic vertical mixing: a review and a model with a nonlocal boundary layer parameterization. Rev Geophys 32:363–403

Leipper DF (1967) Observed ocean conditions and Hurricane Hilda, 1964. J Atmos Sci 24(2):182–186

Lin YL, Chen SY, Hill CM, Huang CY (2005) Control parameters for the influence of a mesoscale mountain range on cyclone track continuity and deflection. J Atmos Sci 62(6):1849–1866

Lin I et al (2003) New evidence for enhanced primary production triggered by tropical cyclone. Geophys Res Lett 30:1718. doi:10.1029/2003GL017141

Lin II, Chen CH, Pun IF, Liu T, Wu CCW (2009) Warm ocean anomaly, air sea fluxes, and the rapid intensification of tropical cyclone Nargis (2008). Geophys Res Lett 36:L03817. doi:10.1029/2008GL035815

Lloyd ID, Vecchi GA (2011) Observational evidence for oceanic controls on hurricane intensity. J Clim 24:1138–1153. doi:10.1175/ 2010JCLI3763.1

Lotliker AA, Kumar TS, Reddem VS, Nayak S (2014) Cyclone Phailin enhanced the productivity following its passage: evidence from satellite data. Curr Sci 106(3):360–361

Mandal M, Singh KS, Balaji M, Mohapatra M (2015) Performance of WRF-ARW model in real-time prediction of Bay of Bengal cyclone 'Phailin'. Pure Appl Geophys. doi:10.1007/s00024-015-1206-7

Maneesha K, Murty VSN, Ravichandran M, Lee T, Yu W, McPhaden MJ (2012) Upper Ocean variability in the Bay of Bengal during the tropical cyclones Nargis and Laila. Prog Oceanogr 106:49–61

Marks F, Shay LK (1998) Landfalling tropical cyclones: forecast problems and associated research opportunities: report of the 5th prospectus development team to the US Weather Research Program. BAMS 79:305–323

Marchesiello P, McWilliams JC, Shchepetkin A (2003) Equilibrium structure and dynamics of the California Current System. J Phys Oceanogr 33(4):753–783

McPhaden MJ, Foltz GR, Lee T, Murty VSN, Ravichandran M, Vecchi GA, Vialard J, Wiggert JD, Yu L (2009) Ocean–atmosphere interactions during cyclone Nargis. EOS Trans AGU 90:53–54. doi:10.1029/ 2009EO070001

Michalakes J, Dudhia J, Gill D, Henderson T, Klemp J, Skamarock W, Wang W (2005) The Weather Research and Forecast Model: software architecture and performance, in: Proceedings of the Eleventh ECMWRF Workshop on the Use of High Performance Computing in Meteorology, Reading, UK, World Scientific 156–168

Mlawer EJ, Taubman SJ, Brown PD, Iacono MJ, Clough SA (1997) Radiative transfer for inhomogeneous atmosphere: RRTM, a validated correlated-k model for the long-wave. J Geophys Res 102:16 663–16 682

Morel A, Antoine D (1994) Heating rate within the upper ocean in relation to its bio-optical state. J Phys Oceanogr 24:1652–1665

Monin AS, Obukhov AMF (1954) Basic laws of turbulent mixing in the surface layer of the atmosphere. Contrib Geophys Inst Acad Sci USSR 151(163):e187

Nayak SR, Sarangi RK, Rajawat AS (2001) Application of IRSP4 OCM data to study the impact of cyclone on coastal environment of Orissa. Curr Sci 80:1208–1213

Neetu S, Lengaigne M, Vincent EM, Vialard J, Madec G, Samson G, Ramesh Kumar MR, Durand F (2012) Influence of oceanic stratification on tropical cyclones-induced surface cooling in the Bay of Bengal. J Geophys Res:117. doi:10.1029/2012JC008433

Noh Y, Cheon WG, Hong SY, Raasch S (2003) Improvement of the K-profile model for the planetary boundary layer based on large eddy simulation data. Bound Layer Meteor 107:401–427

Olabarrieta M, Warner JC, Kumar N (2011) Wave–current interaction in Willapa Bay. J Geophys Res 116:C12014. doi:10.1029/2011JC007387

Olabarrieta M, Warner JC, Armstrong B, He R, Zambon JB (2012) Ocean–atmosphere dynamics during Hurricane Ida and Nor'Ida:

an application of the coupled ocean–atmosphere–wave–sediment transport (COAWST) modeling system. Ocean Model 43–44:112–137. doi:10.1029/2011JC007387

Pant V, Girishkumar MS, Udaya Bhaskar TVS, Ravichandran M, Papa F, Thangaprakash VP (2015) Observed interannual variability of near-surface salinity in the bay of Bengal. J Geophys Res 120(5):3315–3329

Phillips NA (1957) A coordinate system having some special advantages for numerical forecasting. J Met 4:184–185

Piontlovsky SA, Nezlin NP, Al-Azri A, Al-Hashmi K (2012) Mesoscale eddies, and variability of chlorophyll-a in the Sea of Oman. Int J Remote Sens 33(17):5341–5346

Price JF (1981) Upper-ocean response to a hurricane. J Phys Oceanogr 11:153–175

Ricchi A, Miglietta MM, Falco PP, Bergamasco A, Benetazzo A, Bonaldo D, Sclavo M, Carniel S (2016) On the use of a coupled ocean-atmosphere-wave model during an extreme cold air outbreak over the Adriatic Sea. Atmos Res 172–173:48–65. doi:10.1016/j.atmosres.2015.12.023

Riehl H (1950) A model of hurricane formation. J Appl Phys 21(9):917–925

Rao RR, Sivakumar R (2003) Seasonal variability of sea surface salinity and salt budget of the mixed layer of the north Indian Ocean. J Geophys Res 108(C1):3009. doi:10.1029/2001JC000907

Schade LR, Emanuel KA (1999) The ocean's effect on the intensity of tropical cyclones: results from a simple coupled atmosphere-ocean model. J Atmos Sci 56(4):642–651. doi:10.1175/1520-0469

Schade LR (2000) Tropical cyclone intensity and sea surface temperature. J Atmos Sci 57:3122–3130

Sengupta D, Goddalehundi BR, Anitha DS (2007) Cyclone-induced mixing does not cool SST in the post-monsoon north Bay of Bengal. Atmos Sci Lett 9:1–6

Shay LK, Black PG, Mariano AJ, Hawkins JD, Elsberry RL (1992) Upper ocean response to Hurricane Gilbert. J Geophys Res 97(20):227–220

Shay LK, Goni GJ, Black PG (2000) Effects of a warm oceanic feature on Hurricane Opal. Mon Weather Rev 128(5):1366–1383

Shay LK, Brewster JK (2010) Oceanic heat content variability in the eastern Pacific Ocean for hurricane intensity forecasting. Mon Weather Rev 138(6):2110–2131. doi:10.1175/2010MWR3189.1

Shenoi SSC, Shankar D, Shetye SR (2002) Differences in heat budgets of the near-surface Arabian Sea and Bay of Bengal: implications for the summer monsoon. J Geophys Res 107: doi:10.1029/2000JC000679. Issn: 0148–0227.

Skamarock WC, Klemp JB (2008) A time-split non-hydrostatic atmospheric model. J Comput Phys 227:3465–3485

Skamarock WC, Klemp JB, Dudhia J, Gill DO, Barker DM, Wang W, Powers JG (2005) A description of the advanced research WRF version 2. NCAR Technical Note, NCAR/TN-468 + STR

Song Y, Haidvogel D (1994) A semi-implicit ocean circulation model using a generalized topography-following coordinate system. J Comput Phys 115(1):228–244. doi:10.1006/jcph.1994.1189

Stommel H (1958) The abyssal circulation. Deep Sea Res 5:80–82

Subrahmanyam B, Rao KH, Rao NS, Murthy VSN (2002) Influence of a tropical cyclone on chlorophyll-a concentration in the Arabian Sea. Geophys Res Lett 29(22):1–22. doi:10.1029/2002GL015892

Subramanyam B, Murthy VSN, Sharp RJ, O'Brien JJ (2005) Air-sea coupling during the tropical cyclones in the Indian Ocean: a case study using satellite observations. Pure Appl Geophys 162:1643–1672

Subrahmanyam B, Ueyoshi K, Morrison JM (2008) Sensitivity of the Indian Ocean circulation to phytoplankton forcing using an ocean model. Remote Sens Environ 112:1488–1496

Sweeney C, Gnanadesikan A, Griffies S, Harrison M, Rosati A, Samuels B (2005) Impacts of shortwave penetration depth on large-scale ocean circulation heat transport. J Phys Oceanogr 35:1103–1119. doi:10.1175/JPO2740.1

Thadathil P, Muraleedharan PM, Rao RR, Somayajulu YK, Reddy GV, Revichandran C (2007) Observed seasonal variability of barrier layer in the Bay of Bengal. J Geophys Res:112. doi:10.1029/2006JC003651

Tummala SK, Mupparthy RS, Kumar NM, Nayak SR (2009) Phytoplankton bloom due to Cyclone Sidr in the central Bay of Bengal. J Appl Remote Sens 3(1):1–14. doi:10.1117/1.3238329

Venkatesan R, Shamji VR, Latha G, Simi M, Rao RR, Arul M, Atmanand MA (2013) In situ ocean subsurface time-series measurements from OMNI buoy network in the Bay of Bengal. Curr Sci 104(9):1166–1177

Venkatesan R, Mathew S, Vimala J, Latha G, Arul MM, Ramasundaram S, Sundar R, Lavanya R, MA A (2014) Signatures of very severe cyclonic storm Phailin in met–ocean parameters observed by moored buoy network in the Bay of Bengal. Curr Sci 107(4):589–595

Vialard J, Foltz GR, McPhaden MJ, Duvel JP, Montegut CB (2008) Strong Indian Ocean sea surface temperature signals associated with the Madden-Julian Oscillation in late 2007 and early 2008. Geophys Res Lett 35:L19608. doi:10.1029/2008GL035238

Vinayachandran PN, Shankar D, Vernekar S, Sandeep KK, Amol P, Neema CP, Chatterjee A (2013) A summer monsoon pump to keep the Bay of Bengal salty. Geophys Res Lett 40:1777–1782. doi:10.1002/grl.50274

Vincent EM, Lengaigne M, Madec G, Vialard J, Samson G, Jourdain N, Menkes CE, Jullien S (2012a) Processes setting the characteristics of sea surface cooling induced by tropical cyclones. J Geophys Res 117:C02020. doi: 10.1029/2011JC007396

Vincent EM, Lengaigne M, Vialard J, Madec G, Jourdain N, Masson S (2012b) Assessing the oceanic control on the amplitude of sea surface cooling induced by tropical cyclones. J Geophys Res:117. doi: 10.1029/2011JC007705

Walker ND, Leben RR, Balasubramanian S (2005) Hurricane-forced upwelling and chlorophyll a enhancement within cold-core cyclones in the Gulf of Mexico. Geophys Res Lett 32:L18610. doi:10.1029/2005GL023716

Warner JC, Armstrong B, He R, Zambon JB (2010) Development of a coupled ocean–atmosphere–wave–sediment transport (COAWST) modeling system. Ocean Model 35:230–244. doi:10.1016/j. oceanmod.2010.07.010

Warner JC, Armstrong B, Sylvester CS, Voulgaris G, Nelson T, Schwab WC, Denny JF (2012) Storm-induced inner-continental shelf circulation and sediment transport: Long Bay, South Carolina. Cont Shelf Res 42:51–63

Yablonsky RM, Ginis I (2013) Impact of a warm ocean Eddy's circulation on hurricane-Induced Sea surface cooling with implications for hurricane intensity. Mon Weather Rev 141:9971021. doi:10.1175/MWR-D-12-00248.1

Zambon JB, He R, Warner JC (2014) Investigation of hurricane Ivan using the coupled ocean–atmosphere–wave–sediment transport (COAWST) model. Ocean Dyn 64(11):1535–1554

Zhu T, Zhang DL (2006) The impact of the storm-induced SST cooling on hurricane intensity. Adv Atmos Sci 23:14–22